ONLINE FIRST

ISSN: 0015-5659

e-ISSN: 1644-3284

Foramina and canals of the skull base in Holstein cow: a computed tomography study

Authors: Nimet Turgut, Sadullah Bahar, Abidin Kılınçer, Hamza Yavuz Selim Can

DOI: 10.5603/fm.100461

Article type: Original article

Submitted: 2024-04-28

Accepted: 2024-06-06

Published online: 2024-06-10

Foramina and canals of the skull base in Holstein cow: a computed tomography study

Nimet Turgut[1], Sadullah Bahar[1], Abidin Kılınçer[2], Hamza Yavuz Selim Can[1]

[1]Department of Anatomy, Faculty of Veterinary Medicine, Selcuk University, Konya, Türkiye

[2]Department of Radiology, Faculty of Medicine, Selcuk University, Konya, Türkiye

Address for correspondence: Nimet Turgut, Department of Anatomy, Faculty of Veterinary Medicine, Selcuk University, Konya, Türkiye; e-mail: nturgut@selcuk.edu.tr

Abstract

Background: The aim of the study was to describe the comprehensive morphological and morphometric features of the foramina and canals at the base of the cranial cavity in Holstein cow using CT images.

Materials and methods: The study was performed on fourteen adult Holstein cow head cadavers. Images taken with MSCT were transferred to the DICOM Viewer program. The MPR and 3D reconstructive tools of the program were used to analyse the foramina and canals. **Results:** Although they varied in shape and size, foramina and canals were found bilaterally in all animals. It was observed that the orbitorotund foramen, jugular foramen and oval foramen had a canalicular structure, with the distance between the extra-intra cranial openings measured as 15.0 mm, 5.9 mm and 6.2 mm, respectively. The hypoglossal canal, which was found to be single in 43%, double in 50% and triple in 7% in each body half, was the canal with the most variation in number and shape. The orbitorotund foramen, a canal with an area of 180.6 mm^2 and a diameter of 18.1 × 12.4 mm is the widest at the skull base, while the optic canal is the narrowest and longest opening with an area of 33.4 mm^2, a diameter of 8.4 × 5.5 and a length of 17.5 mm.

Conclusions: This study shows that our knowledge of skull base morphometry in animals is extremely limited. Although the study was conducted on a limited number of materials, it may benefit both regional anatomy knowledge in terms of the data presented and veterinary anatomists, radiologists and clinicians in terms of methodology.

Keywords: cattle, cranial fossa, cross section anatomy, morphometry, optic canal

INTRODUCTION

The base of the cranial cavity *(the basis cranii interna*) is divided into three fossae: rostral *(the fossa cranii rostralis*), median *(the fossa cranii media*) and caudal *(the fossa cranii caudalis*). Cranial fossa *(fossa cranii)* contains foramen and canals for the passage of cranial nerves, which show structural changes in animal species [1, 15]. In cattle, rostral cranial fossa contains cribriform plate (*lamina cribrosa*), optic canal (*canalis opticus*, OC), and ethmoidal foramen *(foramen ethmoidale)* on the lateral wall, and middle cranial fossa contains orbitorotund foramen (*foramen orbitorotundum*, ORF) and oval foramen (*foramen ovale*, OF). Caudal cranial fossa contains jugular foramen (*foramen jugulare*, JF), hypoglossal canal (*canalis n. hypoglossi*, HC), and internal auditory canal (*meatus acusticus internus*, IAC) on the lateral wall [32, 45].

The shape, location, relationship with neighboring structures, variations and asymmetric development and morphometric features of the foramina and canals in the cranial fossa on dry skulls or cross-sectional images in people of different ages, genders and races were widely presented [3, 4, 11, 12, 44]. The topographic structure of JF and OF on the dry skull of primates was defined and the diameters of the relevant foramina were measured [6]. The area of JF was determined in the dry skull of bison, macaque, dog, fox and rat [51], and the area of HC was determined in the same species and rabbit [50]. Using CT images, the localization of the chiasmatic sulcus *(sulcus chiasmatis)*, its angle with some bone points [22], and the volume of the JF were determined in the dog [43], and the diameter of the trigeminal nerve canal and OF and the distances between the foramina were measured in the rabbit [20]. Single, double, triple or quadruple HCs were detected in some samples of dog, rhesus monkey, cat, rabbit and rat skulls [34, 50]. As a result, it can be said that studies on the relevant subject in animals are limited in terms of both scope and species. Knowing the size, location and relationships of foramina and canals at the skull base may be important in species and sex determination, zooarchaeology, clinical applications and evaluation of neurological

disorders [35, 37, 42, 43]. Although the general morphological features of the anatomical structures in the base of the cranial cavity in cattle have been described in detail, information about their morphometric features is extremely limited. Veterinary-specific CT devices, which have come into use in the last 10 years, allow imaging of many body parts in large animals, and analysis and clinical evaluations can be made on the images taken from these devices [46]. However, successful evaluation of these images depends on radiological and morphometric information of the relevant region.

The locations of cranial nerves and foramen have been comparatively demonstrated on MRI and CT images in the horse [9, 18], cat [17] and dog [8, 39]. There are very limited studies reporting the morphometric features of these structures in domestic mammals, especially in cattle. There is also no study describing the anatomical features and dimensions of these structures on CT images. The aim of this study is to determine the morphological and morphometric features of the foramina and canals at the base of the cranial cavity by using CT images in Holstein cow and to create normative data.

MATERIALS AND METHODS

Subjects

In the study, 14 female Holstein cow heads (age range, 1.5–8 years) obtained from the slaughterhouse were used. G*Power (version 3.1.9.7) software was used to determine the number of materials (type 1 error probability (alpha) = 0.05, power (1-beta) = 0.80, effect size (dz) = 0.71). The heads of healthy animals were taken after clinical examinations carried out by the slaughterhouse veterinarian. All procedures were carried out with the permission of the Selçuk University Faculty of Veterinary Medicine Experimental Animal Production and Research Center Ethics Committee decision numbered 2022/96.

Computed tomography scans and evaluations

Fourteen heads were scanned perpendicular to the hard palate in the rostrocaudal direction with MSCT (Siemens Dual Source, Somatom Definition Flash, Forheim, Germany) within 24 hours following decapitation (kV: 140, mAs: 475–500, matrix: 512 × 512 and slice thickness: 0.6 mm). The images were evaluated by two authors (XX and XX) with 14 and 16 years of radiological experience, respectively, for compliance with the study criteria (disease,

asymmetric development and anomaly). 0.5 mm axial reformate data sets of 14 animals that met the appropriate criteria for the study were created and archived in Digital Imaging and Communication in Medicine (DICOM) format.

Morphological and morphometric examinations

DICOM data were transferred to a desktop computer with high processing power and screen resolution (4K, 28 inch, Samsung, Suwon, South Korea). RadiAnt DICOM Viewer (Medixant, Poznań, Poland) software was used for morphological evaluation and morphometric parameters. DICOM data sets of each animal were transferred to the program and necessary examinations and measurements were carried out on the images using 3D model tool and the Multiplanar Reconstruction (MPR) tool of the program (Fig. 1–3). In addition, Dicom data were transferred to the MIMICS (Interactive Medical Image Control System, ver: 21.0, Materialise, Leuven, Belgium) program and 3D models of each foramina and canal were created and their morphological structures were evaluated (Fig. 4).

The foramina (ORF, OF, JF) and canals (OC, IAC, HC) at the base of the cranial cavity were evaluated in terms of presence, number, location and shape. In Holstein cow heads, perpendicular maximum diameters and areas of the foramina and canals at the skull base were measured and diameter indices were calculated (Fig. 1D). In foramen measurements, the position of the relevant structure was first determined in the transverse cross-sectional image. Then, planes passing through the center of each of these foramina, parallel and perpendicular to the long axis, were created on sagittal or dorsal plane images. Two perpendicular diameters and areas of the foramina were measured on the narrowest cross-sectional image where the cross-section of the foramen was completely surrounded by bone. In canal measurements, planes parallel and perpendicular to the long axis of the canal were created, and the narrowest point (approximately the middle third) where the canal's cross-section was completely surrounded by 360° bone was determined and the relevant parameters were measured. The area analysis was performed using the freehand tool of the program (bone boundary was drawn by hand) (Fig. 1A–D) [2, 4, 5, 27, 40, 53]. If the foramen or canal was formed more than once, the largest foramen was measured to determine the size. Berlis et al. [4] and Ten et al. [47] were used as reference for angle measurements between the median line and the OC, ORF and OF axis. In this context, angular measurements were made by obtaining dorsal plane CT images of 10° for OC, 0° for ORF, and –30° for OF (Fig 1A-B). While determining the

canal lengths, planes passing through the center of the canal parallel and perpendicular to the long axis were created in the dorsal plane CT images. The first extracranial opening of the canal, surrounded by 360° bones, was determined, and the last intracranial opening of the canal, surrounded by 360° bones, was determined by visualising cross-sections along the backward canal. The distance between these two openings was measured as the canal length (Fig. 1A). In IAC measurement, the distance between the midpoint of the plane passing through the level of the bone walls of the opening of internal auditory canal *(the porus acusticus internus)* and the transverse crest was measured on dorsal plane CT images [4, 53].

All evaluations were performed at a constant contrast, brightness, dim light and bone window setting (window level 300 HU and window width 2800 HU). Measurements were carried out independently by a professor of veterinary anatomy (XX) with 16 years of radiology experience, and after half-day training, by a doctor (XX) with 11 years of anatomy experience, and a PhD student (XX). The measurement of each parameter was repeated three times to minimize measurement error and deviation. Then, statistical analysis was performed by taking the arithmetic mean of these data. Measurement values were defined in millimeters (mm) and presented as mean ± SD. Anatomical structures were named according to classical anatomy books [32, 45] and Nomina Anatomica Veterinaria [31]. Anatomical expressions were given according to English terminology. All anatomical structures were labeled using Adobe Photoshop CC 2015.5 (Adobe system, San Jose, CA, USA).

Statistical analysis

SPSS package program (version 29.0, IBM Corp. Armonk, NY, USA) was used in the statistical analysis of the data obtained in the study. Descriptive statistics (mean, standard deviation, minimum and maximum number) were given for categorical and continuous variables in the study. The assumption of normality was checked by the Shapiro–Wilk test, and the homogenity of variances was checked by the Levene's test. Differences between the parameters of the right and left foramina and canals were determined using Paired-Samples t Test (normally distributed data) and Wilcoxon test (non-normally distributed data). The relationship between two continuous variables was evaluated with Pearson's Correlation Coefficient and, in cases where parametric test prerequisites were not met, with Spearman Correlation Coefficient. $P < 0.05$ and $p < 0.01$ levels were considered statistically significant. 95% confidence intervals of the results of three researchers were calculated to test inter-

researcher reliability (Intraclass Correlation Coefficient (ICC)). Although an ICC above 0.75 is ideal, it is accepted that this coefficient varies between 0 and +1 [26, 29].

RESULTS

In this study, an average of 1066 ± 42 (998-1132) 0.5 mm thick CT section images of 14 female Holstein cows aged between 1.5 and 8 (mean: 5.43 ± 1.69) were analysed. Diameter and area measurements, canal length and angle measurements of a total of 84 foramina and 76 canals were successfully performed on CT images. The parameters of the foramina and canals are presented in Table 1. The relationships between foramina and canals are presented in Table 2. As a result of the examination, ORF, OF, JF, OC, IAC and HC were observed on both sides of the head in all animals, although their shapes and sizes varied (Fig. 2, 3). ICC values of foramina and canals are given in Table 1. In all measurements, inter-researcher agreement was found to be statistically significant ($p < 0.05$). The ICC values of the foramina and canals of the right body half ranged between 0.75 and 0.99 (mean: 0.91), and the values of the left body half ranged between 0.63 and 0.98 (mean: 0.89). ICC values were above 75%, representing perfect agreement in foramen and canal measurements, except for the shorter diameter of internal auditory canal (SDIAC) measurement (0.63, lower bound: 0.17; upper bound: 0.86) (Table 1).

Orbitorotund foramen

The orbitorotund foramen **(**ORF) was in the form of a 15 mm long canal connecting the middle cranial fossa to the pterygopalatine fossa, wide in the rostral and caudal sections and narrower in the middle section, with the dorsol and medial walls shaped by the presphenoid bone and the ventral and lateral walls shaped by the basisphenoid bone (Fig. 2–4). The caudal opening was triangular and the rostral opening was vertical oval shaped. The canal wall was adjacent to the sphenoid sinus (60.7%) medially and the frontal sinus (60.7%) dorsally (Fig. 2a,a’ and 1d). It was determined that this canal reached the orbital floor in the rostrolateral direction, moving away from the median line at an angle of 19.7 ± 2.2° on the right and 20.3 ± 2.5° on the left in the dorsal section. With these dimensions of the canal, which had a diameter of 18.1 × 12.4 mm and an area of 180.6 mm^2, it was the largest opening at the base of the

cranial cavity (Fig. 2, 3). Except for longer diameter of orbitorotund foramen (LDORF) and canal length, all other parameters were observed to be greater on the left ($p < 0.05$) (Table 1).

Oval foramen

The oval foramen (OF) was observed in transverse sections between the wing and pterygoid process of the basisphenoid bone, close to the border of the sphenosquamous sutura, and between the base of the hypophyseal fossa and the dorsum sellae (Fig. 2b,b'). The OF was adjacent to the auditory tube ventromedially. The OF was in the form of an oval-shaped canal, 5.9 mm long, at an angle of 19.6°, symmetrically observed on dorsal plane images (the angles of –30°) (Fig. 1, 4), except in 2 animals (14.3%) (Fig. 2b,b') (Table 1). Consequently, the ORF had a rostro-ventrolateral axis. In 2 animals (140.3–156.7 mm^2), it was observed as a rather larger foramen than the others (Fig. 2b,b'). A positive correlation was observed between longer diameter of oval foramen (LDOF) and shorter diameter of oval foramen (SDOF) ($p = 0.001$, $r = 0.878$) (Table 2).

Jugular foramen

Transverse CT images showed that the jugular foramen (JF) was located at the level of mastoid process. It was in the form of a narrow channel in the middle part, 6.2 mm long, on the petrooccipital synchondroses in the caudal cranial fossa (Fig. 4). The JF was symmetrically located in a rostroventral direction, which was shaped by the jugular notch of 2/5 of the temporal bone and 3/5 of the occipital bone (Fig. 2d,d' and 3b). JF was half-moon-shaped in 85% of the animals and shuttle-shaped in 15%. The intracranial opening of JF's, intracranial opening of internal auditory canal in rostrodorsally was on the same line as HC's intracranial opening in caudoventrally (Fig. 3b). It was observed that the JF opened into the petrooccipital fissure along with the rostrocaudal petrooccipital canal (the canal in sinus petrosus ventralis) (Fig. 2d and 3b). A positive correlation ($p = 0.04$, $r = 0.538$) was detected between longer diameter of jugular foramen (LDJF) and LDORF (Table 2).

Optic canal

The optic canal (OC) were observed to move symmetrically away from each other and reach the orbit in dorsal plane images (the angles of 10°) on the presphenoid bone (Fig. 1, 4). In this images, the angle between the canal and the midline was 42.7 ± 3.3° on the right side and 43.0 ± 2.9° on the left side (Fig. 1b; Table 1). As a result, the OC had a rostro-dorsolateral axis. In images that are perpendicular to this axis, the canal was observed to be dorsoventrally flattened at the beginning (chiasmatic sulcus level) (Fig. 1c) and teardrop-shaped along its entire length rostrally (Fig. 1d, e). It was observed that the OC was separated from the sphenoid (82.1%) and frontal (17.8%) sinuses by a thin bone wall (Fig. 1). With a canal length of 17.5 mm, it was the longest canal at the base of the cranial cavity (Table 1). A positive correlation was found between index of optic canal (OCI) and index of orbitorotund foramen (ORFI) ($p = 0.03$, r: 0.559).

Internal auditory canal

The internal auditory canal (IAC) was a canal with an intracranial opening *(the porus acusticus internus)* located in the middle partion of the medial surface of the petrous part. In the paramedian sections, the opening of IAC was in the shape of a half-moon and a triangle, and in the lateral sections, the canal narrowed and extended to the transverse crest (Fig. 3B). It was observed that the right and left the opening of IAC were positioned opposite to each other in the transverse section (Fig. 2, 4). In the dorsal, transverse and paramedian cross-sectional examinations, the rostral facial canal located at the base of the canal and the ventrolateral area cochlea and laterodorsal area vestibularis superior were clearly observed (Fig. 2c, c'). Morphometric data of the canal are shown in Table 1. Shorter diameter of internal auditory canal (SDIAC) and index of internal auditory canal (IACI) were found to be greater on the left ($p < 0.05$). IAC was similar to HC with a canal length of 7.8 mm (Table 1).

Hypoglossal canal

The hypoglossal canal (HC) connecting the caudal cranial fossa and the ventral condyloid fossa showed the most variation in number and shape (Fig. 2e, e'). It was determined that it consisted of a single bilateral canal in 4 animals, a double canal on the right and a single canal on the left in 2 animals, a single canal on the right and a double canal on the left in 2 animals, a double bilateral canals in 5 animals, and three bilateral canals in 1 animal (Fig. 3, 4). It was observed that the most caudal canal in all animals examined had a larger diameter than the others. In 3 animals, it was observed as a rather large opening due to the dorsal junction of the

canal with the condylar canal. Diameter, area and length were not measured in these animals. The results of morphometric analyses of the canal are shown in Table 1. A positive correlation was observed between shorter diameter of hypoglossal canal (SDHC) and longer diameter of hypoglossal canal (LDHC) ($p = 0.001$, $r = 0.961$) (Table 2).

DISCUSSION

This study provided a comprehensive description of the morphological and morphometric features of the foramina and canals in the base of the cranial cavity in cattle, which have not been previously described in the veterinary literature. All morphometric analyses in the study were performed by three different researchers and the results were presented as mean ± SD. As a result of ICC, it was determined that all values were above 0.75 except the SDIAC. This data shows that the morphometric analyses were repeatable (Table 1). In the current study, shorter diameter of orbitorotund foramen (SDORF), area of orbitorotund foramen (AORF), ORFI and ORF angle were found to be larger on the left in opening measurements, and SDIAC and IACI in canal measurements ($p < 0.05$) (Table 1). In the base of the cranial cavity, the longest canal with the smallest diameter and cross-sectional area was OC, and the opening with the largest diameter and cross-sectional area was ORF. OF had the shortest canal length. Morphologically, HC was the most asymmetrical canal (Fig. 2e,e' and 3b), and OC was the most symmetrical canal in terms of right and left dimensions. It was observed that ORF (pre-basisphenoid bones) and JF (occipital and temporal bones) were formed between two bones within the basal foramen (Fig. 2 and 3).

In cattle, the ORF has been defined as a large foramen located at the junction of the basisphenoid bone and the presphenoid bone (middle cranial fossa) [1, 32]. This foramen, which is present in pigs and ruminants, has been described in classical sources [1, 21, 32] as the equivalent of the f round foramen, orbital fissure and trochlear foramen in the horse. In deer (Hippocamelus bisulcus), the ORF is divided into two compartments, dorsal and ventral [33]. In the present study, the ORF was observed as a smooth-walled canal with a triangular intracranial opening and a vertical oval orbital opening, bounded by the pre-basisphenoid bone as described in the literatüre (Fig. 2a and 3a). It was the largest opening at the base of the cranial cavity with a length of 15.0 mm, a diameter of 18.1 × 12.4 mm and a cross-sectional area of 180.6 mm^2, neighbouring the sphenoid and frontal sinus (Fig. 2a, a' and 3a). The ORF was found to be larger on the left in terms of some morphometric data (Table 1).

Similar asymmetry was reported in the round foramen in humans [3]. In morphometric studies on humans, the foramina at the base of the cranial cavity were described as canal-like when the distance between the intra- and extracranial walls exceeded 2 mm [14, 44]. We believe that the ORF, which is narrow in the middle part and has a wider opening in the caudal and rostral parts, can be defined as a canal in Holstein cattle (Fig. 2, 4).

In humans, the OF is located in the middle cranial fossa, behind the wing of the sphenoid bone. Although the foramen has different shapes such as round, semicircular, pear, almond, slit, irregular, etc., the most common shape is oval [11, 44]. It has been reported that the OF can sometimes be double shaped and sometimes partially divided by a bone curtain [4]. In the New Zealand rabbit, a positive correlation ($r = 0.54$) was found between the diameter of the OF and body weight [20]. In the dog, the OF was described as a large opening that directly leaves the cranial cavity, caudolateral to the round foramen, anterior to the basisphenoid bone [15, 45]. In the horse and pig, it was defined as the notch (incisura) on the caudal edge of the basisphenoid bone, lateral to the foramen lacerum. In ruminants, it was described as a single large foramen located at the base of the basisphenoid bone [21, 32]. Hillmann [21] reported that the OF in sheep is slightly rostral compared to its position in cattle. In our study, the OF observed in transverse sections at the level of dorsum sella was symmetrical ($p > 0.05$), smooth-walled and oval with a diameter of 11.3 × 7.4 mm and an area of 69.4 mm^2 (Table 1). The OF was observed as a rostro-ventrolateral directed canal with a length of 5.9 ± 1.5 mm in 12 (85.7%) animals (Fig. 1, 4) and as a wide opening in 2 (14.3%) animals (Fig. 2b, b’), much larger than the average (18.4 × 10.4 mm, 148.5mm^2) compared to other animals. There was no correlation between the OF and other morphometric data except its own measurements (Table 2). Our results regarding the location and shape of the OF are generally compatible with the literature.

The JF is located ventrolateral to the caudal cranial fossa and provides the passage of the vagus group nerves and some vascular structures. The formation of this foramen, located caudal to the petrooccipital fissure, shows some differences between humans and domestic mammals. In horse and pig, this fissure is wide. Therefore, it is called foramen lacerum. In these species, caudally of foramen lacerum is also called jugular foramen (JF) or foramen lacerum aborale. In carnivores and ruminants, this fissure is narrow, its rostral end forms the petrooccipital canal (the canal of the sinus petrosus ventralis) and its caudal end forms the JF [1, 10, 15, 31, 32]. In carnivores and ruminants, JF is formed by the combination of the jugular notch of the occipital and temporal bones [10, 25, 31]. In humans, the JF is an

irregular foramen divided into two compartments known as the pars nervosa anteriorly and the pars vascularis posteriorly by a bony protrusion extending between the temporal or occipital bones [36, 49]. A similar condition has been shown in primates [6] and in the Mongrel dog, rat and macaque [51]. In the present study, the JF was observed as half-moon (85%) or shuttle-shaped with smooth walls, which were formed by the jugular notch of 2/5 the temporal bone and 3/5 of the occipital bone (Fig. 2d, d' and 3b), in accordance with those reported for Cattle. Contrary to what was reported in human, primate, dog and rat, no bone protrusion was observed dividing the opening intracranial JF. In European bison (n = 67), the area of the JF was determined to be 45.6 mm^2 on the right and 51.2 mm^2 on the left in females, while it was 47.2 mm^2 on the right and 51.3 mm^2 on the left in males. In the Holstein breed, these values were measured as 76.5 and 74.1 mm^2 on the right and left, respectively. The observation of an approximately 50% difference between two species of the *Bovidae* family may be due to the size difference of the species and may be largely due to the methodological difference used in the studies.

In domestic mammals, OC is the canal between the chiasmatic sulcus and the optic foramen in the rostral cranial fossa where the optic nerve and the accompanying meninges and internal ophthalmic artery are located [21, 25, 32]. The chiasmatic sulcus, where the intracranial openings of the canal are located, is deep in equus and ruminant, but quite shallow in carnivores [32]. In the rabbit, the OC and chiasmatic sulcus are replaced by a large foramen that communicates with both orbits simultaneously [1]. In humans, the OC is an asymmetrically shaped canal in the middle cranial fossa, in the upper part of the sphenoid bone body, extending towards the orbital wall, adjacent to the sphenoid sinus [4, 49]. Bekerman et al. [2] reported that the lumen of the canal in adults is usually circular, sometimes oval or triangular, with a mean length of 7.82 mm and across-sectional area of 6.6–25.5 mm^2. In a CT study of 335 individuals, the mean canal length was determined as 5.61 mm, diameter 3.28 mm, and cross-sectional area 11.84 mm^2 [53]. In another study using CT images, the mean maximum-minumum diameter and cross-sectional area in the middle part of the OC were measured as 5.1 × 3.97 mm and 15.78 mm^2, respectively [41]. In the present study, the intracranial opening of the canal was dorsoventrally flattened (Fig. 1c) and the apex was observed as a medially directed teardrop along its rostral course (Fig. 1e). The canal was adjacent to the sphenoid sinus (if present) and frontal sinus (Fig. 1). The canal diameters, length and area measurements in Holstein cow were 8.4 × 5.5, 17.5 mm and 33.4 mm^2, respectively (Table 1). The results of the study show that the OC in Holstein cow is

morphologically similar to humans and morphometrically higher than humans. Ichikawa et al. [22] reported that the angle between the optic chiasma and the right-left lacrimal–zygomatic joint was 93.74° in brachycephalic dogs, 67.87° in mesocephalic dogs, and 61.05° in dolichocephalic dogs. In humans, Ten et al. [47] reported the angle between OC and median plane as 39.3°, Berlis et al. [4] 39.1°, Cheng et al., [7] 45.3° (right), 44.2° (left), Zhang et al. [52] 43.2°, Park et al. [38] 39.9°. In cattle, the angle between the OC (AngOC) and the midline axis (42.9°) can be said to be similar to humans (Table 1).

In domestic mammals, the IAC is a short canal with an opening called the porus acusticus internus at the level of the medial surface of the petrous part and terminates with a blind end (the fundus meatus acusticus internus). Cranial nerves (VII-VIII) course within the canal [21, 25, 32]. Barone [1] reported that the IAC is relatively narrow in the horse and its opening has a triangular shape, whereas in the donkey it is less deep and its opening is oval shaped. In humans, it is a cylindrical, bud and funnel shaped canal, usually symmetrically located [3, 24]. In the present study, the opening of IAC *(the porus acusticus internus)* was observed as triangular or half-moon shaped in paramedian sections (Fig. 3b). Kobayashi and Zusho [24] reported the posterior wall length of the IAC as 8.7 mm on radiographs in humans, and El Sadik and Shaaban [13] reported the canal length as 7.00 mm on CT images. In another study [4] performed on axial and coronal CT images, canal lengths were measured as 10.38 and 11.98 mm, respectively. The results of this study using 14 animals show that Holstein cows and humans are similar in terms of canal length (Table 1).

In domestic mammals, the HC is formed in the lateral part of the occipital bone, between the paracondylar process and occipital condyle, and connects the cranial cavity to the ventral cranial fossa. The canal contains the nerve of the same name, the emissary ven and the condylar artery except the carnivore. The HC has been described as a single canal represented by a large foramen in the horse, usually double in cattle, and sometimes double in sheep and goats [1, 21, 32]. Wysocki et al. [50] reported that this canal is formed as double in 43% of humans, 36% in monkeys, 12% in dogs, 14% in cats, 7% in rats, 69% in rabbits and single in foxes and bison. Uddin et al. [48] reported that 80% of cats and Olude et al. [34] reported that 87% of African giant rats had two or more canals. In the present study, it was observed that 43% of the skulls had single, 50% had double and 7% had three canals (Fig. 3, 4). Our study results show that HC has significant variation in terms of number and shape in this species, as in other species. In the present study, the canal length was measured as 8.0 and 7.1 mm on the right and left, respectively (Table 1). Right and left canal lengths were reported as 8.67 and

8.26 mm in Italian population [19], 8.89 and 9.03 mm in Greek population (p = 0.046) [28], 12.6 mm in Indian population [30], 10.0 and 9.8 mm in Turkish population [23], 7.78 mm in European skulls [4]. Our study results show that humans and Holstein cows are morphometrically similar except for the Indian population.

In the present study, the HC diameter measurements were performed with two perpendicular measurements from the middle and narrowest part of the canal length as in other canals. These values, called longer and shorter diameters, were found to be 9.7 × 7.4 and 10.2 × 7.8 mm (mean 9.9 × 7.6 mm) on the right and left, respectively. In a study using similar methodology, these values were reported as 4.5 × 4.24 mm in humans [4]. In the same study, the intra-extracranial opening diameter values of the canal were measured as 9.08 × 6.85 and 9.08 × 6.95, respectively [4]. Berge and Bergman [3] reported the intra-extracranial opening diameters of the HC in humans as 5.51 × 4.25 and 4.66 × 3.21 mm, respectively. In some studies, intra-extracranial diameter values were given as a single value on the right and left. These values were reported as 6.12 and 6.39 mm in Italian population [19], 7.2 and 7.9 mm in Indian population, 6.14 and 6.11 mm in Egyptian skulls [16], 6.5 and 6.6 mm in Turkish population [23]. In the above studies on the skull, canal mophometry was mostly evaluated by showing extracranial and inracranial opening diameters. In humans, the HC is shown to be an important canal involved in the venous drainage of the brain next to the hypoglassal nerve. Therefore, the narrowest part of the canal should be taken as a reference in the morphometric evaluation of this canal. We think that it would be more accurate to evaluate the canal with CT studies as in Berlis et al. [4]. Wysocki et al. [50] reported that the cross-sectional area of HC was larger in European bison males (right-left: 49.7–48.6 mm^2) than in females (42.1–42.9 mm^2) and that there was a positive relationship between this data and cranial capacity. In Holstein cow, the cross-sectional area of the HC was 20% higher in male bison and 50% higher in female bison (Table 1). This may be due to differences in species and the method used.

Limitations of the study include the use of females of limited age and number belonging to a single species, the extremely limited morphometric data available for domestic mammals, and the lack of a comprehensive methodology for determining the morphometric features of these foramina and canals, including human studies.

CONCLUSIONS

A round or cylindrical anatomical structure can be accurately measured in any plane. However, due to the different shapes of the foramina and canals at the skull base, it is difficult to make accurate, reliable and repeatable measurements in the axial plane. CT is always considered the gold standard for morphological and morphometric evaluation of the external and internal structure of complex anatomical structures such as the skull. Despite some limitations, our study focused on determining the variations and morphometric features (diameter, length, angle, area) of the foramina and canals at the skull base in Holstein cow. The first detailed reference data of the relevant structures at the skull base were presented with a repeatable measurement protocol using CT images. Our findings may be useful to anatomists, radiologists, clinicians and other researchers in neuroanatomy, neuropathology and zooarchaeology.

Article information and declarations

Data availability statement

The data that support the findings of this study are available from the corresponding author upon reasonable request.

Ethics statement

All procedures were carried out with the permission of the Selçuk University Faculty of Veterinary Medicine Experimental Animal Production and Research Center Ethics Committee decision numbered 2022/96.

Author contributions

All authors contributed to the conception and design of the study. Material acquisition and preparation was performed by [Nimet Turgut]. The optimised CT settings and acquired CT data were performed by [Abidin Kılınçer], and the CT data were reviewed by [Sadullah Bahar] and [Abidin Kılınçer]. Morphological evaluation and morphometric analysis were performed by [Sadullah Bahar] and [Nimet Turgut] and [Hamza Yavuz Selim Can]. The definition of all anatomical structures and the visualisation of the figures were carried out by [Sadullah Bahar] and [Nimet Turgut]. Statistical analyses and preparation of tables were

carried out by [Nimet Turgut]. The first draft of the manuscript was written by [Nimet Turgut] and [Sadullah Bahar], and all authors have commented on previous versions of the manuscript.

Funding

The authors declare no sources of funding forthe work presented here.

Acknowledgments

Preliminary findings of a part of the investigation, the abstract, were presented in “2nd International cappadocia scientific research congress, June 17–19, 2022/Cappadocia-Nevşehir”. The authors would like to thank the Radiology Department of Selcuk University for helping them to obtain the images.

Conflict of interest

The authors declare no conflicts of interest or sources of funding forthe work presented here.

REFERENCES

1. Barone R. Anatomie comparee des mammiferes domestiques: Tome I Osteologie. Vigot Freres, Paris 1999.
2. Bekerman I, Kimiagar I, Sigal T, et al. Monitoring of intracranial pressure by CT-defined optic nerve sheath diameter. J Neuroimaging. 2016; 26(3): 309–314, doi: 10.1111/jon.12322, indexed in Pubmed: 26686547.
3. Berge JK, Bergman RA. Variations in size and in symmetry of foramina of the human skull. Clin Anat. 2001; 14(6): 406–413, doi: 10.1002/ca.1075, indexed in Pubmed: 11754234.
4. Berlis A, Putz R, Schumacher M. Direct and CT measurements of canals and foramina of the skull base. Br J Radiol. 1992; 65(776): 653–661, doi: 10.1259/0007-1285-65-776-653, indexed in Pubmed: 1393389.

5. Bidot S, Clough L, Saindane AM, et al. The Optic Canal Size Is Associated With the Severity of Papilledema and Poor Visual Function in Idiopathic Intracranial Hypertension. J Neuroophthalmol. 2016; 36(2): 120–125, doi: 10.1097/WNO.0000000000000318, indexed in Pubmed: 26580295.

6. Bold J, Szemet M, Goździewska-Harłajczuk K, et al. Topography of cranial foramina and anaesthesia techniques of cranial nerves in selected species of primates (Cebidae, Cercopithecidae, Lemuridae) - part I - osteology. BMC Vet Res. 2023; 19(1): 122, doi: 10.1186/s12917-023-03680-7, indexed in Pubmed: 37573315.

7. Cheng Ye, Liu M, Zhang S, et al. Optic canal (OC) and internal carotid artery (ICA) in sellar region. Surg Radiol Anat. 2013; 35(9): 797–801, doi: 10.1007/s00276-013-1193-2, indexed in Pubmed: 24005376.

8. Couturier L, Degueurce C, Ruel Y, et al. Anatomical study of cranial nerve emergence and skull foramina in the dog using magnetic resonance imaging and computed tomography. Vet Radiol Ultrasound. 2005; 46(5): 375–383, doi: 10.1111/j.1740-8261.2005.00068.x, indexed in Pubmed: 16250393.

9. Dixon J, Lam R, Weller R, et al. Clinical application of multidetector computed tomography and magnetic resonance imaging for evaluation of cranial nerves in horses in comparison with high resolution imaging standards. Equine Vet Educ. 2016; 29(7): 376–384, doi: 10.1111/eve.12629.

10. Dyce KM, Sack WO, Wensing CJG. Textbook of veterinary anatomy. 2nd edition. W.B.Saunders Company, New York 1996.

11. Edwards B, Wang JMh, Iwanaga J, et al. Cranial Nerve Foramina Part I: A Review of the Anatomy and Pathology of Cranial Nerve Foramina of the Anterior and Middle Fossa. Cureus. 2018; 10(2): e2172, doi: 10.7759/cureus.2172, indexed in Pubmed: 29644159.

12. Edwards B, Wang JMh, Iwanaga J, et al. Cranial Nerve Foramina: Part II - A Review of the Anatomy and Pathology of Cranial Nerve Foramina of the Posterior Cranial Fossa. Cureus. 2018; 10(4): e2500, doi: 10.7759/cureus.2500, indexed in Pubmed: 29928560.

13. El Sadik AO, Shaaban MH. The relationship between the dimensions of the internal auditory canal and the anomalies of the vestibulocochlear nerve. Folia Morphol. 2017; 76(2): 178–185, doi: 10.5603/FM.a2016.0052, indexed in Pubmed: 27665959.

14. Elnashar A, Patel SK, Kurbanov A, et al. Comprehensive anatomy of the foramen ovale critical to percutaneous stereotactic radiofrequency rhizotomy: cadaveric study of dry skulls. J Neurosurg. 2019; 132(5): 1414–1422, doi: 10.3171/2019.1.JNS18899, indexed in Pubmed: 31003215.

15. Evans HE, Christensen GC. Miller's anatomy of the dog. 2nd edition. W.B Saunders Company, Tokyo 1979.

16. Farid SA. Morphometric Study of Human Adult Occipital Condyle, Hypoglossal Canal and Foramen Magnum in Dry Skull of Modern Egyptians. International Journal of Clinical and Developmental Anatomy. 2018; 4(1): 19, doi: 10.11648/j.ijcda.20180401.13.

17. Gomes E, Degueurce C, Ruel Y, et al. Anatomic study of cranial nerve emergence and associated skull foramina in cats using CT and MRI. Vet Radiol Ultrasound. 2009; 50(4): 398–403, doi: 10.1111/j.1740-8261.2009.01556.x, indexed in Pubmed: 19697605.

18. Gonçalves R, Malalana F, McConnell JF, et al. ANATOMICAL STUDY OF CRANIAL NERVE EMERGENCE AND SKULL FORAMINA IN THE HORSE USING MAGNETIC RESONANCE IMAGING AND COMPUTED TOMOGRAPHY. Vet Radiol Ultrasound. 2015; 56(4): 391–397, doi: 10.1111/vru.12256, indexed in Pubmed: 25832323.

19. Guarna M, Lorenzoni P, Franci D, et al. Hypoglossal canal: an osteological and morphometric study on a collection of dried skulls in an Italian population: clinical implications. Eur J Med Res. 2023; 28(1): 501, doi: 10.1186/s40001-023-01489-6, indexed in Pubmed: 37941031.

20. Herta J, Wang WT, Höftberger R, et al. An experimental animal model for percutaneous procedures used in trigeminal neuralgia. Acta Neurochir (Wien). 2017; 159(7): 1341–1348, doi: 10.1007/s00701-017-3162-8, indexed in Pubmed: 28397136.

21. Hillmann DJ. Skull. In: Getty R. ed. Sisson and Grossman's the anatomy of the domestic animals. W.B Saunders Company, Tokyo 1975: 318–1253.

22. Ichikawa Y, Kanemaki N, Kanai K. Breed-Specific Skull Morphology Reveals Insights into Canine Optic Chiasm Positioning and Orbital Structure through 3D CT Scan Analysis. Animals (Basel). 2024; 14(2), doi: 10.3390/ani14020197, indexed in Pubmed: 38254367.

23. Kizilkanat E, Boyan N, Soames R, et al. Morphometry of the Hypoglossal Canal, Occipital Condyle, and Foramen Magnum. Neurosurgery Quarterly. 2006; 16(3): 121–125, doi: 10.1097/01.wnq.0000214018.49915.49.

24. Kobayashi H, Zusho H. Measurements of internal auditory meatus by polytomography. 1. Normal subjects. Br J Radiol. 1987; 60(711): 209–214, doi: 10.1259/0007-1285-60-711-209, indexed in Pubmed: 3567465.

25. König HE, Liebich HG. Veterinary anatomy of domestic mammals: Textbook and colour atlas. 6th edition. Schattauer GmbH 2004.

26. Lee J, Koh D, Ong CN. Statistical evaluation of agreement between two methods for measuring a quantitative variable. Comput Biol Med. 1989; 19(1): 61–70, doi: 10.1016/0010-4825(89)90036-x, indexed in Pubmed: 2917462.

27. Li S, Liao C, Qian M, et al. Narrow ovale foramina may be involved in the development of primary trigeminal neuralgia. Front Neurol. 2022; 13: 1013216, doi: 10.3389/fneur.2022.1013216, indexed in Pubmed: 36303558.

28. Lyrtzis Ch, Piagkou M, Gkioka A, et al. Foramen magnum, occipital condyles and hypoglossal canals morphometry: anatomical study with clinical implications. Folia Morphol. 2017; 76(3): 446–457, doi: 10.5603/FM.a2017.0002, indexed in Pubmed: 28150268.

29. McGraw K, Wong SP. Forming inferences about some intraclass correlation coefficients. Psychological Methods. 1996; 1(1): 30–46, doi: 10.1037/1082-989x.1.1.30.

30. Muthukumar N, Swaminathan R, Venkatesh G, et al. A morphometric analysis of the foramen magnum region as it relates to the transcondylar approach. Acta Neurochir (Wien). 2005; 147(8): 889–895, doi: 10.1007/s00701-005-0555-x, indexed in Pubmed: 15924208.

31. Nomina Anatomica Veterinaria. International committee on veterinary gross anatomical nomenclature. 2017.

32. Nickel R, Schummer A, Seiferle E. The locomotor system of the domestic mammals. Verlag Paul Parey, Berlin 1986.

33. Núñez-Cook S, Vidal Mugica F, Salinas P. Skull anatomy of the endangered Patagonian huemul deer(Hippocamelus bisulcus). Anat Histol Embryol. 2022; 51(6): 728–739, doi: 10.1111/ahe.12851, indexed in Pubmed: 35946781.

34. Olude MA, Olopade JO, Fatola IO, et al. Some aspects of the neurocraniometry of the African giant rat (Cricetomys gambianus Waterhouse). Folia Morphol. 2009; 68(4): 224–227, indexed in Pubmed: 19950071.

35. Onar V, Çakirlar C, Janeczek M, et al. Skull typology of Byzantine dogs from the Theodosius Harbour at Yenikapi, Istanbul. Anat Histol Embryol. 2012; 41(5): 341–352, doi: 10.1111/j.1439-0264.2012.01143.x, indexed in Pubmed: 22372748.

36. Ong CK, Fook-Hin Chong V. Imaging of jugular foramen. Neuroimaging Clin N Am. 2009; 19(3): 469–482, doi: 10.1016/j.nic.2009.06.007, indexed in Pubmed: 19733318.

37. Parés-Casanova PM. Basicranial analysis in young bovines reveals a relation to breed and sex. Anat Histol Embryol. 2013; 42(5): 398–401, doi: 10.1111/ahe.12019, indexed in Pubmed: 23198864.

38. Park SJ, Yoo JN, Yoo MS, et al. A study on double angle of optic foramen in the Rhese method. J Korean Soc Radiol. 2017; 11: 313–319, doi: 10.7742/jksr.2017.11.5.313.

39. Parry AT, Volk HA. Imaging the cranial nerves. Vet Radiol Ultrasound. 2011; 52(1 Suppl 1): S32–S41, doi: 10.1111/j.1740-8261.2010.01783.x, indexed in Pubmed: 21392154.

40. Pircher A, Montali M, Berberat J, et al. The Optic Canal: A Bottleneck for Cerebrospinal Fluid Dynamics in Normal-Tension Glaucoma? Front Neurol. 2017; 8: 47, doi: 10.3389/fneur.2017.00047, indexed in Pubmed: 28280481.

41. Pirinc B, Fazliogullari Z, Koplay M, et al. Morphometric and morphological evaluation of the optic canal in three different parts in MDCT images. Int Ophthalmol. 2023; 43(8): 2703–2720, doi: 10.1007/s10792-023-02670-w, indexed in Pubmed: 36890419.

42. Saito T, Nemoto T, Nagase Y, et al. Development of a stereotaxic instrument for study of the bovine central nervous system. Brain Res Bull. 2004; 62(5): 369–377, doi: 10.1016/j.brainresbull.2003.07.010, indexed in Pubmed: 15168901.

43. Schmidt MJ, Ondreka N, Sauerbrey M, et al. Volume reduction of the jugular foramina in Cavalier King Charles Spaniels with syringomyelia. BMC Vet Res. 2012; 8: 158, doi: 10.1186/1746-6148-8-158, indexed in Pubmed: 22954070.

44. Šink Ž, Umek N, Alibegović A, et al. Sphenoidal Foramen Ovale in the Slovenian Population: An Anatomical Evaluation with Clinical Correlations. Diagnostics (Basel). 2023; 13(5), doi: 10.3390/diagnostics13050962, indexed in Pubmed: 36900106.

45. Sisson S. Skull. In: Getty R. ed. Sisson and Grossman's the anatomy of the domestic animals. W.B Saunders Company, Tokyo 1975: 762–1503.

46. Stewart HL, Siewerdsen JH, Nelson BB, et al. Use of cone-beam computed tomography for advanced imaging of the equine patient. Equine Vet J. 2021; 53(5): 872–885, doi: 10.1111/evj.13473, indexed in Pubmed: 34053096.

47. Ten B, Beger O, Esen K, et al. Anatomic features of the cranial aperture of the optic canal in children: a radiologic study. Surg Radiol Anat. 2021; 43(2): 187–199, doi: 10.1007/s00276-020-02604-6, indexed in Pubmed: 33130955.

48. Uddin M, Sarker M, Hossain ME, et al. Morphometric investigation of neurocranium in domestic cat (Felis catus). Bangladesh Journal of Veterinary Medicine. 2014; 11(1): 69–73, doi: 10.3329/bjvm.v11i1.17302.

49. Williams PL, Warwick R, Dyson M. Gray's anatomy. 3rd edition. Churchill Livingstone, New York 1989.

50. Wysocki J, Kobryń H, Bubrowski M, et al. The morphology of the hypoglossal canal and its size in relation to skull capacity in man and other mammal species. Folia Morphol. 2004; 63(1): 11–17, indexed in Pubmed: 15039894.

51. Wysocki J. Morphology of the temporal canal and postglenoid foramen with reference to the size of the jugular foramen in man and selected species of animals. Folia Morphol. 2002; 61(4): 199–208.

52. Zhang H, Liu X, Cheng Ye, et al. A new method of locating the optic canal based on structures in sella region: computed tomography study. J Craniofac Surg. 2013; 24(3): 1011–1015, doi: 10.1097/SCS.0b013e318287d228, indexed in Pubmed: 23714935.

53. Zhang X, Lee Y, Olson D, et al. Evaluation of optic canal anatomy and symmetry using CT. BMJ Open Ophthalmol. 2019; 4(1): e000302, doi: 10.1136/bmjophth-2019-000302, indexed in Pubmed: 31245611.

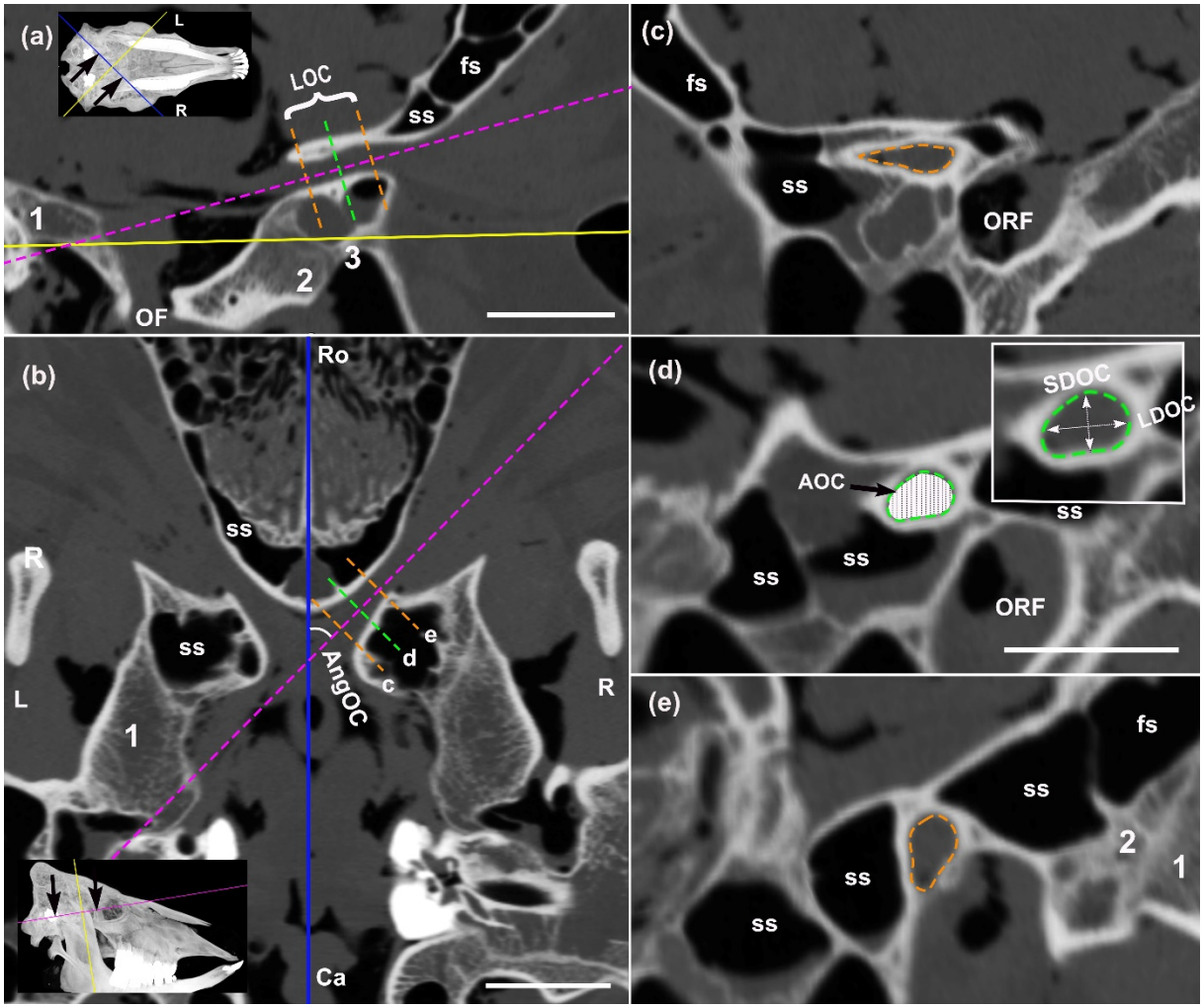

Figure 1. The optic canal and its morphometric measurements (No:7, 3.5 years old). **A.** Transcanalicular sagittal oblique section CT image (straight yellow line: dorsal line, pink dashed line: transcanalicular line) **B.** Dorsal section CT image at angle of 10° (pink dashed line: transcanalicular line, straight blue line: midsagittal line). **C.** Intracranial opening of the

right optic canal. **D.** Middle portion of the right optic canal (diameter and area measurements were performed in this section). **E.** Extracranial opening of the right optic canal. AngOC — Angle of the optic canal; AOC — area of optic canal; fs, frontal sinus; LDOC — longer diameter of optic canal; LOC — length of optic canal; ORF — orbitorotund foramen; OF — oval foramen; SDOC — shorter diameter of optic canal; ss — sphenoid sinus; 1, temporal bone; 2, basisphenoid bone; 3, presphenoid bone. Ca — cranial; R — right; Ro — rostral; L — left. Scale bars: 3 cm. The images are taken from the multiplanar reconstruction of the RadiAnt DICOM Viewer software.

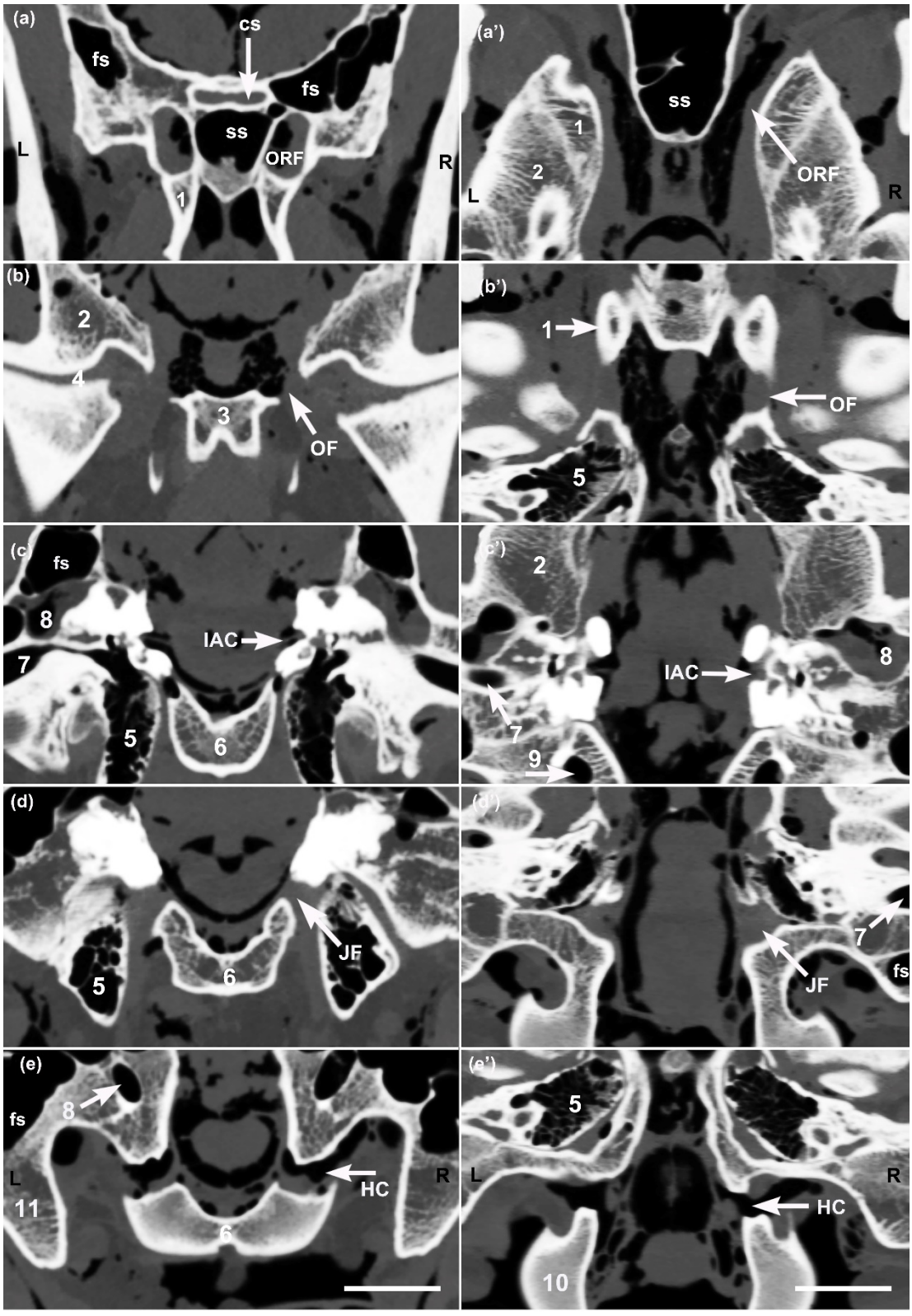

Figure 2. Foramina and canals in transverse (**A–E**) and dorsal (**A'–E'**) CT section images (No: 4, 5 years old). HC — hypoglossal canal; IAC — internal auditory canal; JF — jugular foramen; ORF — orbitorotund foramen; OF — oval foramen; cs — chiasmatic sulcus; fs —

frontal sinus; ss — sphenoid sinus; 1 — basisphenoid bone; 2 — temporal bone; 3 — body of the basisphenoid bone; 4 — temporomandibular joint; 5 — tympanic bulla; 6 — basilar part of the occipital bone; 7 — external auditory canal; 8 — temporal meatus; 9 — condylar canal; 10 — occipital condyle of the occipital bone; 11 — paracondylar process of the occipital bone. R — right; L — left. Scale bars: 3 cm. The images are taken from the multiplanar reconstruction of the RadiAnt DICOM Viewer software.

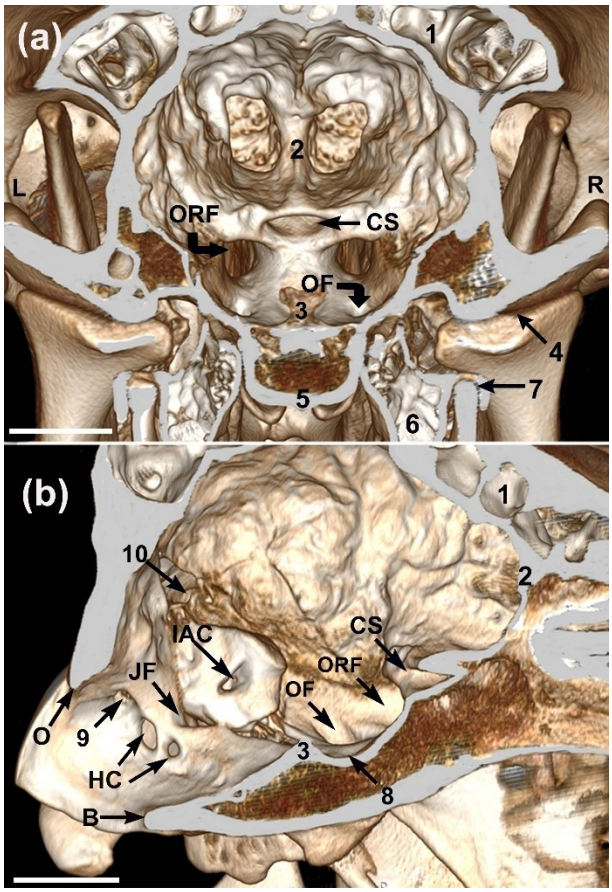

Figure 3. Foramina and canals on 3D skull section models (No: 11, 5 years old). **A.** Caudorostral view (at the level of the temporomandibular joint). **B.** Left mediolateral view. CS — chiasmatic sulcus; B — basion; HC — hypoglossal canal; IAC — internal auditory canal; JF — jugular foramen; O — opisthion; ORF — orbitorotund foramen; OF — oval foramen; 1, frontal sinus; 2, ethmoidal crest; 3, dorsum sellae, 4, temporomandibular joint; 5, body of the basisphenoid bone; 6, tympanic bulla; 7, temporohyoid joint; 8, hypophyseal

fossa; 9, condylar canal; 10, temporal meatus. R — right; L — left. Scale bars: 3 cm. The images are taken from the 3D model (3D VR) of the RadiAnt DICOM Viewer software.

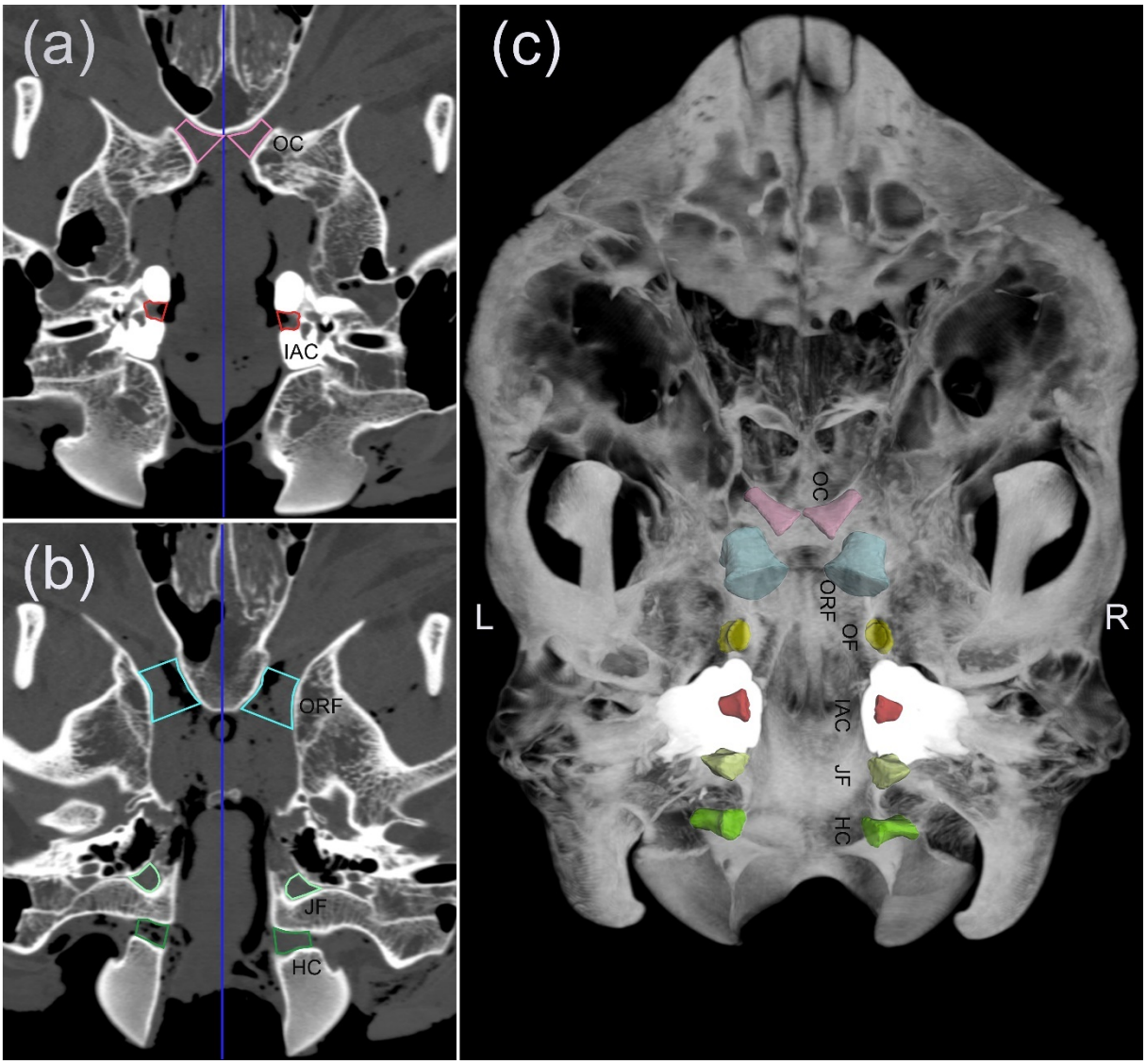

Figure 4. 3D model images of foramina and channels (No:10, 6 years old). **A.** Dorsal section CT image. **B.** Dorsal section CT image. **C.** Dorsal reconstructive image of the skull base. CT — computed tomography; OC — Optic canal; ORF — orbitorotund foramen; OF — oval foramen; IAC — internal auditory canal; JF — jugular foramen; HC — hypoglossal canal. The images are taken from the multiplanar reconstruction and 3D screen of the MIMICS software.

Morphometric features of the canals and the foramina in Holstein cows (n = 14)

Parameters	Mean ± SD		Total Mean ± SD		Minumum–Maximum		I
Foramens and canals (mm–mm^2)	Right	Left	Right and Left	*P*	Right	Left	Right
Foramen							
Orbitorotundum							
Longer diameter (LDORF)	18.0 ± 1.3	18.1 ± 1.6	18.1 ± 1.4	0.565$^{\lambda}$	16.6–20.6	16.2–21.3	0.94 (0.85–0.9
Shorter diameter (SDORF)	12.2 ± 1.2	12.6 ± 1.2	12.4 ± 1.2	**0.001***$^{\lambda}$	10.1–14.1	10.7–14.6	0.89 (0.70–0.9
Index (ORFI)	67.8 ± 7.3	70.2 ± 7.7	68.0 ± 7.3	**0.016***$^{\lambda}$	56.1–79.6	56.2–80.4	
Length of canal	15.2 ± 2.6	15.0 ± 3.1	15.0 ± 2.8	0.652$^{\lambda}$	9.3–19.67	7.5–19.6	0.97 (0.92–0.9
Area (AORF)	177.4 ± 21.1	183.8 ± 22.2	180.6 ± 21.1	**0.035***$^{\varepsilon}$	136.9–201.2	138.6–209.2	0.94 (0.80–0.9
	19.7 ± 2.2	20.3 ± 2.5	20.0 ± 2.3	**0.031***$^{\lambda}$	14.2–23.2	14.4–24.1	0.97 (0.91–0.9
Longer diameter (LDOF)	11.2 ± 3.2	11.3 ± 3.2	11.3 ± 3.2	0.638$^{\varepsilon}$	8.0–19.2	8.1–20.4	0.99 (0.98–0.9
Shorter diameter (SDOF)	7.3 ± 1.6	7.5 ± 1.4	7.4 ± 1.5	0.193$^{\lambda}$	5.7–10.9	5.3–10.4	0.99 (0.98–0.9
Index (OFI)	67.0 ± 8.5	68.3 ± 10.8	67.7 ± 8.6	0.605$^{\lambda}$	54.4–85.2	50.9–87.6	
Length of canal	5.5 ± 1.4	6.3 ± 1.6	5.9 ± 1.5	0.050$^{\lambda}$	3.4–7.7	4.6–9.9	0.99 (0.97–0.9
Area (AOF)	67.5 ± 35.0	71.3 ± 35.8	69.4 ± 34.9	0.209$^{\varepsilon}$	36.7–152.7	40.2–171.0	0.99 (0.99–0.9
	19.8 ± 2.8	19.5 ± 2.8	19.6 ± 2.7	0.366$^{\lambda}$	14.8–24.8	15.1–25.1	0.95 (0.89–0.9
Longer diameter(LDJF)	13.1 ± 1.3	12.9 ± 1.1	13.0 ± 1.2	0.165$^{\lambda}$	10.7–15.7	11.1–14.5	0.95 (0.89–0.9
Shorter diameter (SDJF)	7.8 ± 0.9	7.7 ± 0.8	7.8 ± 0.8	0.463$^{\lambda}$	6.6–9.6	6.1–8.9	0.84 (0.61–0.9
Index (JFI)	59.8 ± 7.3	59.6 ± 5.3	59.7 ± 6.0	0.730$^{\varepsilon}$	51.0–80.3	52.0–72.2	
Length of canal	6.4 ± 1.2	6.1 ± 1.3	6.2 ± 1.2	0.372$^{\lambda}$	4.3–8.9	4.2–9.1	0.99 (0.99–0.9
Area (AJF)	76.5 ± 14.1	74.1 ± 13.1	75.3 ± 13.1	0.259$^{\lambda}$	53.9–107.23	52.4–93.8	0.96 (0.90–0.9
Longer diameter (LDOC)	8.4 ± 0.4	8.4 ± 0.5	8.4 ± 0.4	0.869$^{\lambda}$	7.7–9.2	7.6–9.2	0.80 (0.53–0.9
Shorter diameter (SDOC)	5.5 ± 0.4	5.5 ± 0.4	5.5 ± 0.4	0.571$^{\lambda}$	5.0–6.5	4.9–6.3	0.89 (0.75–0.9
Index (OCI)	65.5 ± 4.9	65.9 ± 5.8	65.7 ± 4.8	0.759$^{\lambda}$	58.4–77.9	55.2–75.7	
Length of canal (LOC)	17.5 ± 1.9	17.5 ± 2.0	17.5 ± 1.9	0.923$^{\lambda}$	13.8–19.8	14.0–20.3	0.91 (0.79–0.9
Area (AOC)	33.5 ± 3.1	33.3 ± 3.5	33.4 ± 3.2	0.730$^{\lambda}$	28.7–39.8	28.0–41.8	0.88 (0.72–0.9
)(AngOC)	42.7 ± 3.3	43.0 ± 2.9	42.9 ± 3.1	0.127$^{\lambda}$	34.2–49.0	35.8–47.8	0.98 (0.97–0.9
Internal auditory							
Longer diameter (LDIAC)	9.3 ± 0.9	9.4 ± 0.9	9.4 ± 0.8	0.746$^{\lambda}$	8.3–11.2	8.2–11.2	0.86 (0.66–0.9

Shorter diameter (SDIAC)	5.7 ± 0.8	6.1 ± 0.7	5.9 ± 0.7	**0.043*$^{\lambda}$**	3.7–6.8	4.6–7.2	0.75 (0.35–0.9
Index (IACI)	61.8 ± 10.3	65.5 ± 7.7	63.7 ± 8.7	**0.024*$^{\lambda}$**	42.2–80.2	51.5–81.7	
Length of canal	7.8 ± 1.0	7.8 ± 0.8	7.8 ± 0.9	0.643$^{\lambda}$	6.0–9.3	6.3–9.1	0.97 (0.93–0.9
Area (AIAC)	40.5 ± 7.2	43.4 ± 6.5	42.0 ± 6.4	0.051$^{\lambda}$	25.9–52.2	32.1–52.5	0.81 (0.51–0.9
Hypoglossal							
Longer diameter (LDHC)	9.7 ± 1.2	10.2 ± 2.0	9.9 ± 1.5	0.382$^{\lambda}$	6.8–11.6	7.5–13.5	0.91 (0.66–0.9
Shorter diameter (SDHC)	7.4 ± 1.3	7.8 ± 1.3	7.6 ± 1.2	0.079$^{\lambda}$	6.1–10.5	6.6–10.6	0.97 (0.90–0.9
Index (HCI)	76.6 ± 8.5	77.3 ± 8.2	76.9 ± 8.2	0.992$^{\lambda}$	66.6–90.3	61.5–89.1	
Length of canal	8.0 ± 2.1	7.1 ± 1.7	7.6 ± 1.9	0.608$^{\lambda}$	4.5–11.0	4.7–10.2	0.99 (0.97–0.9
Area (AHC)	58.0 ± 17.6	62.9 ± 23.0	60.2 ± 19.8	0.211$^{\lambda}$	33.2–101.2	37.1–110.2	0.98 (0.90–0.9

*p < 0.05 $^{\lambda}$Paired sample t–test, $^{\epsilon}$Wilcoxon Test. Index = shorter diameter/Longer diameter*100. (Right HC, n = 11; Left HC, n = 9) (Length of canal of OF, N
AHC — area of hypoglossal canal; AIAC — area of internal auditory canal; AJF — area of jugular foramen; AngOC — angle of the optic canal; AOC — area
area of oval foramen; AORF — area of orbitorotund foramen; CI — confidence interval; HCI — index of hypoglossal canal; IACI — index of internal audito
correlation coefficient; JFI — index of jugular foramen; LDHC — longer diameter of hypoglossal canal; LDIAC — longer diameter of internal auditory canal
diameter of jugular foramen; LDOC — longer diameter of optic canal; LDOF — longer diameter of oval foramen; LDORF — longer diameter of orbitorotund
of optic canal; OCI — index of optic canal; OFI — index of oval foramen; ORFI — index of orbitorotund foramen; SDHC — shorter diameter of hypoglossal
diameter of internal auditory canal; SDJF — shorter diameter of jugular foramen; SDOC — shorter diameter of optic canal; SDOF — shorter diameter of oval
shorter diameter of orbitorotund foramen.

Table 2. The relationship between diameter and area measurements of foramina and canals (n = 14)

	LDORF	SDORF	LDOF	SDOF	LDJF	SDJF	LDOC	SDOC	LDIAC	SDIAC	LDHC
AORF	,767**	,727**									
SDOF			,878**								
AOF			,989**	,928**							
LDJF	,538*										
AJF					,870**	,861**					
AOC							,606*	,766**			
AIAC									,816**	,649*	
SDHC											,961*
AHC											,928*

*, $p < 0.05$; **, $p < 0.01$ (Right HC, n = 11; Left HC, n = 9).

AHC — area of hypoglossal canal; AIAC — area of internal auditory canal; AJF — area of jugular foramen; area of optic canal; AOF — area of oval foramen; AORF — area of orbitorotund foramen; LDHC — longer d hypoglossal canal; LDIAC — longer diameter of internal auditory canal; LDJF — longer diameter of jugular LDOC — longer diameter of optic canal; LDOF — longer diameter of oval foramen; LDORF — longer diam orbitorotund foramen; SDHC — shorter diameter of hypoglossal canal; SDIAC — shorter diameter of interna canal; SDJF — shorter diameter of jugular foramen; SDOC — shorter diameter of optic canal; SDOF — sho diameter of oval foramen; SDORF — shorter diameter of orbitorotund foramen.